The University of Sydney

Department of Civil Engineering
Sydney NSW 2006
AUSTRALIA

http://www.civil.usyd.edu.au/

Environmental Fluids/Wind Group

A three-dimensional numerical model for wave-induced soil response around the head of a breakwater

Research Report No R859

Dong-Sheng Jeng, BE ME PhD
Jian Li BSc MSc PhD

December 2005

The University of Sydney

Department of Civil Engineering
Environmental Fluids/Wind Group
http://www.civil.usyd.edu.au/

A three-dimensional numerical model for wave-induced soil response around the head of a breakwater

Research Report No R859

Dong-Sheng Jeng, BE ME PhD
Jian Li, BSc MSc PhD

December 2005

Abstract:

The evaluation of wave-induced seabed response has been recognised as a dominant factor in analyzing the seabed instability in the vicinity of a breakwater. Most previous investigations for wave-induced pore water pressure have been limited to two-dimensions, which are not able to simulate the phenomenon around the head of a breakwater. In this study, a three-dimensional model for the wave-induced pore pressure around the head of a breakwater is established for both oscillatory and residual mechanisms. Numerical results conclude: (1) diffracted wave components significantly affect the distribution of pore water pressure and vertical effective normal stresses and liquefaction potential; (2) a liquefied hole occurs near the head of a breakwater; (3) incident wave angles do not only affect the pattern of liquefied regions, but also the maximum liquefaction depth; (4) the soil types significantly affect the distribution of soil response and liquefaction, and liquefaction only occurs in fine sand, not coarse sand.

Keywords:
pore pressure, vertical effective normal stresses, marine sediment, breakwater, liquefaction

Copyright Notice

Department of Civil Engineering, Research Report R859
A three-dimensional numerical model for wave-induced soil response around the head of a breakwater

d.jeng@civil.usyd.edu.au j.li@civil.usyd.edu.au

Published by:
Department of Civil Engineering
The University of Sydney
Sydney NSW 2006
AUSTRALIA

December 2005

This report and other Research Reports published by The Department of Civil Engineering are available on the Internet:

http://www.civil.usyd.edu.au

Contents

1 Introduction

Protection of the coastal environment is vital for countries like Australia, where more than 80% of the total population is concentrated in coastal regions. Marine structures such as offshore breakwaters are commonly adopted for such protection. Design of marine structures considering their stability is a rather complicated problem. One of important factors which have to be taken into considerations in the design procedure is the wave-induced seabed instability (liquefaction) in the vicinity of the structures. It has been well documented that ocean waves propagating over the ocean surface exert dynamic pressure fluctuations on the sea floor. These fluctuations generate an excess pore pressure within the soil skeleton, which have been recognized as a dominant factor in analyzing the seabed instability. Recently, some marine structures have been reported to be damaged by seabed instability at their toes (Silvester and Hsu, 1989). Furthermore, it has been observed that a deep hole exists near the tip of a marine structure (Sumer and Fredsøe, 2002). Without proper maintenance at these sites, failure of structures may be expected.

In general, the wave phenomenon in the vicinity of a marine structure contains two types of wave system, occurring in front of and at the tip of the structure (Figure 1). When waves arrive obliquely at a marine structure (zone A), the portions of the crests are reflected from the wall. In this region, the incident waves will interact with their reflected waves, the resulting in a short-crested wave system propagating along the breakwater. When the waves arrive at the tip of a marine structure in region B, the reflected waves are diffracted due to the discontinuity of the structure at the tip. Thus, the total wave is a combination of incident, reflected and diffracted waves. Because the reflected wave components do not exit in zone C, the wave system is a combination of incident and diffracted waves. Furthermore, only diffracted wave components exist in region D.

Two mechanisms of the wave-induced seabed response have been reported in the literature (see Figure 2), depending upon how the excess pore pressure is generated (Nago et al., 1993). One is caused by the residual or progressive nature of the excess pore pressure, which appears in the initial stage of cyclic loading. This type of soil response is similar to that induced by earthquakes, caused by the build-up of excess pore pressure (Seed and Rahman, 1978). The other, generated by transient

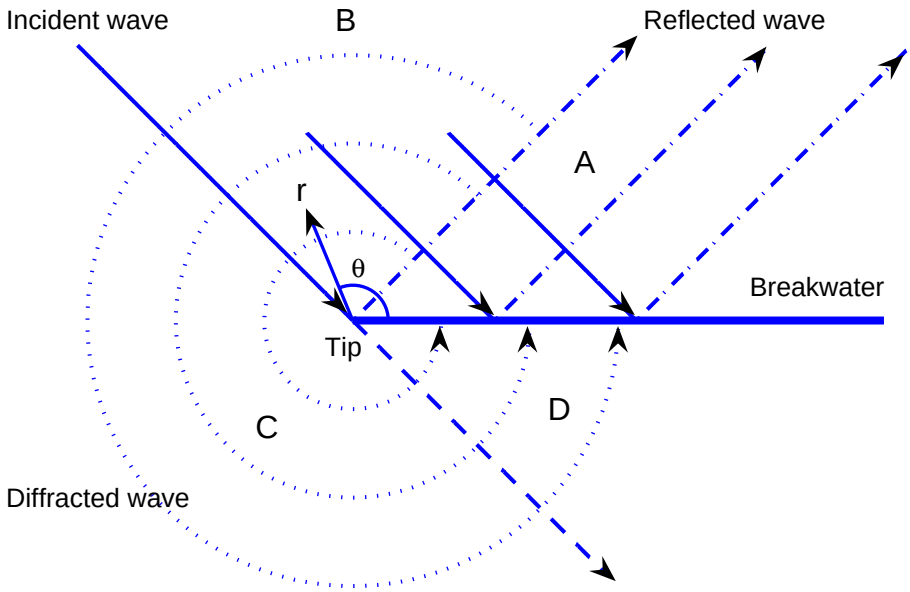

(a) wave field around a breakwater

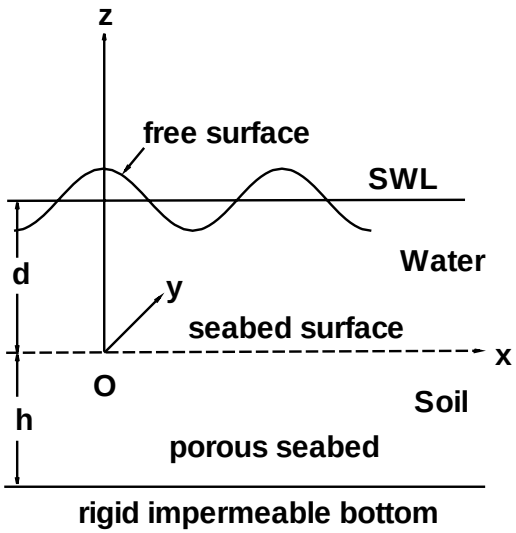

(b) wave-seabed-structure interaction

Figure 1: Sketch of wave-seabed interaction in the vicinity of a breakwater. (a) wave field around a breakwater, and (b) wave-seabed-structure interaction.

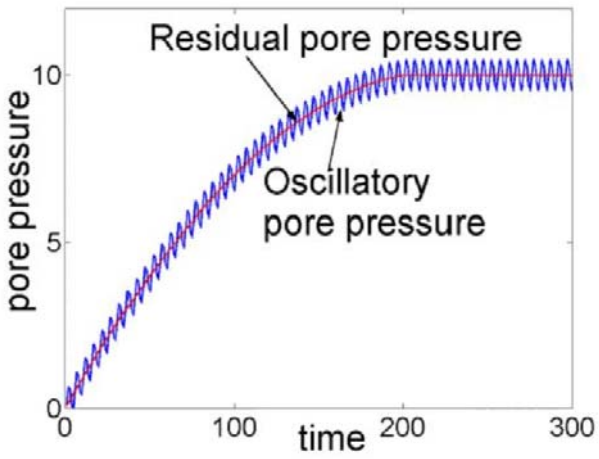

Figure 2: Mechanisms of wave-induced pore pressure in marine sediments.

or oscillatory excess pore pressures, is accompanied by the damping of amplitude and phase lag in the pore pressure, and appears as a periodic response to each wave (Yamamoto et al., 1978; Madsen, 1978; Jeng, and Hsu, 1996). In this study, both mechanisms will be considered.

As shown in Figure 2, the wave-induced pore water pressure in marine sediments consists of two components: Transient (oscillatory) and residual (build-up) mechanisms. Thus, the wave-induced pore pressure can be expressed as

$$p = \widetilde{p} + \overline{p}, \tag{1}$$

where p represents the wave-induced pore water pressure, $\widetilde{p}$ is the transient pore pressure, and $\overline{p}$ is the residual pore pressure, which is defined by

$$\overline{p} = \frac{1}{T}\int_{t}^{t+T} p dt, \tag{2}$$

in which T is the wave period.

Numerous investigations for the wave-induced seabed response, including pore pressure, effective stresses and soil displacements, have been carried out since the

1970's. Among these, analytical approximations (Madsen, 1978; Jeng, 1997), numerical modeling (Thomas, 1989, 1995; Jeng, 2003a; Sassa et al. 2001) and experimental work (Tsui and Helfrich, 1983; Tsai and Lee 1995, Sassa and Sekiguchi, 1999) have been adopted to investigate the wave-induced oscillatory pore pressure and momentary liquefaction in marine sediments. The contributions and limitation of previous studies in the area have been systematically reviewed in Jeng (2003b). However, all previous models have been limited to either one-dimensional or two-dimensional case, which can only represent part of the whole problem (i.e., Zone A in Figure 1).

Jeng (1996) appears to be the unique study to investigate the wave-induced pore pressure and liquefaction at the tip of a breakwater. In his analytical model, only transient soil response in an infinite seabed was considered in the model. However, realistic seabed mostly are porous medium of finite thickness. Therefore, the model cannot provide a complete understanding of the whole problem. In addition, a mistake is found in one of the governing equations used in his model, as mentioned in the next section. Thus, the results are doubtable, and it is desire to establish a model with correct governing equations.

Residual mechanisms of wave-induced pore pressure have been investigated since Seed and Rahman (1978). Dynamic wave pressures that vary harmonically in space and time will generate cyclic shear stresses in the soil that can cause the contraction of relatively loose soils and in turn lead to an increase in the mean excess pore water pressure if drainage is impeded. These mean pore pressures are not uniquely related to instantaneous values of the wave-induced stresses, but depend on the accumulated action of the cyclic loading and the rate of pore pressure dissipation. Under this action, liquefaction may develop in un-drained or poorly drained conditions. Some recent investigations of this mechanism were carried out by McDougal et al. (1989); Sumer and Cheng (1999), Cheng et al. (2001), Sassa and Sekiguchi (1999) and Sumer and Fredsøe (2002).

In summary, the gaps between the previous investigations and proposed study are:

(a) Most previous investigations have only considered the wave-induced seabed response in front of a breakwater, rather than at the tip of a breakwater, although the latter is more important for engineering design.

(b) The existing studies for the wave-induced soil response at the tip of a breakwater only consider transient soil response in a infinite seabed with an incorrect governing equation. Thus, a better model for more realistic case of finite thickness is desired.

(c) The existing model for wave-induced residual pore pressure have been limited to one-dimensional model, which cannot handle the case around the head of a breakwater.

In this study, a set of three-dimensional governing equation for both oscillatory and residual pore pressure around the head of a breakwater will be established first. A finite difference model will then be established to investigate the wave-induced pore pressure and effective stresses in a porous seabed around the head of a breakwater. With the new numerical model, the influence of dominant factors on the wave-induced pore pressure will be examined.

2 Transient (Oscillatory) Mechanism

2.1 Governing equations

[1]The problem modelled in this study is depicted in Figure 1. With the assumptions of compressible pore fluid and soil and poro-elasticity, the wave-induced oscillating soil response is governed by Biot's consolidation equation (Biot, 1941), i.e.,

$$K\left(\frac{\partial^2\widetilde{p}}{\partial r^2}+\frac{1}{r}\frac{\partial\widetilde{p}}{\partial r}+\frac{1}{r^2}\frac{\partial^2\widetilde{p}}{\partial\theta^2}+\frac{\partial^2\widetilde{p}}{\partial z^2}\right)-n_e\beta_0\gamma_w\frac{\partial\widetilde{p}}{\partial t}=\gamma_w\frac{\partial\varepsilon}{\partial t}, \tag{3}$$

where p is the wave-induced pore pressure, K, n_e, β_0 and ε are soil permeability, soil porosity, compressibility of soil and volumetric strain, respectively. G is shear modulus, and μ is Poisson's ratio. The compressibility of soil (β_0) and the volumetric strain (ε) are defined by

$$\varepsilon=\varepsilon_{rr}+\varepsilon_{\theta\theta}+\varepsilon_{zz}\quad\text{and}\quad\beta_0=\frac{1}{K'}+\frac{1-S}{P_{wo}}, \tag{4}$$

in which ε_{rr}, $\varepsilon_{\theta\theta}$ and ε_{zz} are the strain in the r-, θ- and z-directions, respectively [defined in (11)-(13], $K'=2\times10^9$ N/m^2, S is the degree of saturation, and $P_{wo}=\gamma_w d$ (d is the water depth, γ_w is the unit weight of pore fluid).

Based on poro-eastic theory, The stress-strain relationship can be expressed as

$$\sigma'_r=2G(\varepsilon_{rr}+\frac{\mu\varepsilon}{1-2\mu}), \tag{5}$$

$$\sigma'_\theta=2(\varepsilon_{\theta\theta}+\frac{\mu\varepsilon}{1-2\mu}), \tag{6}$$

$$\sigma'_z=2G(\varepsilon_{zz}+\frac{\mu\varepsilon}{1-2\mu}), \tag{7}$$

[1]Part of this section form the manuscript: Jeng and Li (2005): A three-dimensional numerical model for wave-induced transient pore pressure around the head of a a breakwater. International Journal of Oceans and Oceanography (accepted)

$$\tau_{r\theta} = 2G\varepsilon_{r\theta}, \tag{8}$$

$$\tau_{rz} = 2G\varepsilon_{rz}, \tag{9}$$

$$\tau_{\theta z} = 2G\varepsilon_{\theta z}, \tag{10}$$

where

$$\varepsilon_{rr} = \frac{\partial u_r}{\partial r}, \qquad \varepsilon_{\theta\theta} = \frac{u_r}{r} + \frac{\partial u_\theta}{\partial \theta}, \qquad \varepsilon_{zz} = \frac{\partial u_z}{\partial z}, \tag{11}$$

$$\varepsilon_{r\theta} = \frac{1}{r}\frac{\partial u_r}{\partial \theta} + \frac{\partial u_\theta}{\partial r} - \frac{u_\theta}{r}, \tag{12}$$

$$\varepsilon_{\theta z} = \frac{1}{r}\frac{\partial u_z}{\partial \theta} + \frac{\partial u_\theta}{\partial z}, \tag{13}$$

$$\varepsilon_{rz} = \frac{\partial u_r}{\partial z} + \frac{\partial u_z}{\partial r}. \tag{14}$$

The equations for force balance can be expressed as

$$\frac{1}{r}\frac{\partial (r\sigma'_r)}{\partial r} - \frac{\sigma'_\theta}{r} + \frac{1}{r}\frac{\partial \tau_{r\theta}}{\partial \theta} + \frac{\partial (\tau_{rz})}{\partial z} = \frac{\partial \widetilde{p}}{\partial r}, \tag{15}$$

$$\frac{1}{r}\frac{\partial (r\sigma'_\theta)}{\partial \theta} + \frac{1}{r}\frac{\partial \tau_{\theta z}}{\partial z} + \frac{1}{r^2}\frac{\partial (r\tau_{r\theta})}{\partial \theta} = \frac{1}{r}\frac{\partial \widetilde{p}}{\partial \theta}, \tag{16}$$

$$\frac{\partial \sigma'_z}{\partial z} + \frac{1}{r}\frac{\partial (r\tau_{rz})}{\partial r} + \frac{1}{r}\frac{\partial \tau_{\theta z}}{\partial \theta} = \frac{\partial \widetilde{p}}{\partial z}. \tag{17}$$

Substituting (5)-(10) into (15)-(17), we have

$$2G\left\{\nabla^2 u_r + \frac{1-\mu}{1-2\mu}\frac{\partial \varepsilon}{\partial r} - \frac{1}{r}\frac{\partial}{\partial r}\left(r\frac{\partial u_r}{\partial r}\right) - \frac{1}{r^2}\frac{\partial u_\theta}{\partial \theta}\right\} = \frac{\partial \widetilde{p}}{\partial r}, \tag{18}$$

$$2G\left\{\nabla^2 u_\theta + \frac{1-\mu}{1-2\mu}\frac{\partial \varepsilon}{\partial \theta} + \frac{1}{r^2}\frac{\partial u_r}{\partial \theta} - \frac{u_\theta}{r^2} - \frac{1}{r^2}\frac{\partial^2 u_\theta}{\partial \theta^2}\right\} = \frac{1}{r}\frac{\partial \widetilde{p}}{\partial \theta}, \tag{19}$$

$$2G\left\{\nabla^2 u_z + \frac{1-\mu}{1-2\mu}\frac{\partial \varepsilon}{\partial z} - \frac{\partial^2 u_z}{\partial z^2}\right\} = \frac{\partial \widetilde{p}}{\partial z}. \tag{20}$$

It is noted that "$1/r$" on the right-hand-side of (19) was missing in Jeng (1996), which is corrected here.

2.2 Boundary conditions

To solve the above governing equations, (3), (18)-(20), appropriate boundary conditions are required. First, the wave-induced pore pressure equals to wave dynamic pressure at the surface of the seabed, and vertical effective normal stress and shear stresses vanish, i.e.,

$$\widetilde{p} = P_b, \quad \sigma_z' = \tau_{rz} = \tau_{\theta z} = 0 \qquad \text{at} \quad z = 0 \tag{21}$$

where dynamic wave pressure at the surface of the seabed is given by (Stoker, 1957),

$$P_b = p_0 \sum_{m=0}^{\infty} e^{-i\omega t} e^{-im\pi/4} \varepsilon_m J_{m/2}(kr) \cos\left(\frac{m\alpha}{2}\right) \cos\left(\frac{m\theta}{2}\right), \tag{22a}$$

$$p_0 = \frac{H_i}{2\cosh kd}, \qquad \varepsilon_m = \begin{Bmatrix} 1 & m = 0 \\ 2 & m \neq 0 \end{Bmatrix} \tag{22b}$$

in which α is the incident wave angle, and $J_{m/2}$ is the first-kind of Bessel function with $m/2$-th order.

Second, the soil displacements and pressure gradient vanish at the seabed bottom, i.e.,

$$u_r = u_\theta = u_z = \frac{\partial \widetilde{p}}{\partial z} = 0 \qquad \text{at} \quad z = -h \tag{23}$$

Third, assumming the breakwater is a rigid structure, which leads to impermeable boundary conditions at both sides of walls, i.e.,

$$\frac{\partial p}{\partial n} = \sigma_n = 0 \ \text{ along } \ \theta = 0 \ \text{ and } \ \theta = 2\pi. \tag{24}$$

in which ϵ_{rr}, $\epsilon_{\theta\theta}$ and ϵ_{zz} are the strain in the $r-$, $\theta-$ and $z-$directions, respectively; $K' = 2 \times 10^9$ N/m^2, and $P_{wo} = \gamma_w d$ (d is the water depth, γ_w is the unit weight of pore fluid).

2.3 Numerical scheme

In this study, we use the finite difference method to solve the equation (3), (18)-(20) numerically. Suppose that all solutions are periodic and have the form $e^{-i\omega t}$ for the time t. The nodes and step sizes Δr, $\Delta\theta$ and Δz are defined by

$$\begin{aligned} &\Delta r = L/N, \ \ \Delta\theta = 2\pi/M, \ \ \Delta z = h/J, \\ &r_n = n\Delta r,\ n = 0, \cdots, N; \\ &\theta_m = m\Delta\theta, m = 0, \cdots, M; \\ &z_j = j\Delta z, j = 0, \cdots, J. \end{aligned} \tag{25}$$

where N, M and J are the mesh in the r-, θ- and z-directions, respectively.

Let $p_m^{n,j}$ denote the value of $\widetilde{p}$ at the (r_n, θ_m, z_j)-th node. The finite difference scheme of equation (3) is constructed as follows

$$\begin{aligned} &\frac{p_m^{n+1,j} - 2p_m^{n,j} + p_m^{n-1,j}}{\Delta r^2} + \frac{1}{r_n}\frac{p_m^{n+1,j} - p_m^{n-1,j}}{2\Delta r} \\ &+\frac{1}{r_n^2}\frac{p_{m+1}^{n,j} - 2p_m^{n,j} + p_{m-1}^{n,j}}{\Delta\theta^2} + \frac{p_m^{n,j+1} - 2p_m^{n,j} + p_m^{n,j-1}}{\Delta z^2} \\ &+ \frac{in_e\beta\gamma_w\omega}{K_z}p_m^{n,j} = -\frac{i\gamma_w\omega}{K_z}\varepsilon_m^{n,j}. \end{aligned} \tag{26}$$

The Neumann boundary conditions are approximated by the use of a second-order accurate formulae. Then we get the following equation

$$A_p p = f_p(u_r, u_\theta, u_z). \tag{27}$$

Similarly, (18)-(20) can be re-written as

$$A_{u_r} u_r = f_{u_r}(\widetilde{p}, u_\theta, u_z), \tag{28a}$$
$$A_{u_\theta} u_\theta = f_{u_\theta}(\widetilde{p}, u_r, u_z), \tag{28b}$$
$$A_{u_z} u_z = f_{u_z}(\widetilde{p}, u_r, u_\theta). \tag{28c}$$

In the iterative procedures, successive overrelaxation (SOR) is first used to solve the equations (27)-(28c) separately. We use $\omega_{SOR}(0 < \omega_{SOR} < 2)$ to denote relaxation parameter and it may be different for the equations (27)-(28c). Second, under-relaxation is employed in order to obtain convergent solutions. Let ω_{UR} be relaxation parameter and ϵ_c the criteria for the iterative procedure to converge. In our computation, we take $\epsilon_c = 10^{-8}$. For example, the iterative solution of equation we obtain $u_r^{(k+1)}$ from the equation (28a) if

$$|u_r^{(k+1)} - u_r^{(k)}| < \epsilon_c, \tag{29}$$

and then the iterative procedure is terminated, otherwise the new $(k+1)$-th value which is introduced into the next iteration is given by

$$u_r^{(k+1)} = \omega_{UR} u_r^{(k+1)} + (1 - \omega_{UR}) u_r^{(k)}, \tag{30}$$

where $0 < \omega_{UR} \leq 1$.

2.4 Results and discussion

The effects of wave and soil characteristics on the wave-induced pore pressure and effective stresses in marine sediments have been discussed in the previous work with two-dimensional models (Jeng, 1997). Thus, the objectives of this paper are to examine the influence of factors, which only exist in three-dimensional cases, such as diffracted wave components and incident wave angles, on the wave-induced pore

Table 1: Input data for numerical examples.

Wave characteristics	
Wave period (T)	12.0 sec
Water depth (d)	20 m
Wave length (L)	112.27 m
Wave height (H)	10 m
Soil characteristics	
seabed thickness (h)	25 m
Poisson's ratio (μ)	0.333
Soil porosity (n_e)	0.3
Shear modulus (G)	10^7 or 5×10^6 N/m^2
Soil permeability (K)	10^{-2}, 10^{-4} or 10^{-6} m/sec
Unit weight of soil (γ_s)	2.65 γ_w
Unit weight of pore fluid (γ_w)	9806 N/m^3

pressure and effective stresses around the head of a breakwater. The input data for numerical examples are tabulated in Table 1. In our numerical procedure, we take ω_{SOR}=1.4 or 1, ω_{UR}=0.01, N=25, M=32 and J=20. To simplify the expression of oscillatory pore pressure in the figures, p is used instead of $\widetilde{p}$ in all illustrations in this section.

2.4.1 Diffracted waves

The major differences between the present 3-D and previous 2-D models are the consideration of wave diffraction, which only occurs near the head of a breakwater. The contour distributions of the non-dimensional wave-induced pore pressure ($\widetilde{p}/p_o$) at soil depth $z = -1$ m at different time intervals is illustrated in Figures 3-6. Since we focus on the region near the head of a breakwater, we only present the results within $r/L = 1$. In the figure, the incident wave angle is 135 degrees ($\alpha = 3\pi/4$). As shown in the figure, the wave troughs move from north-west direction (i.e., $\theta = 3\pi/4$) at $t/T = 0$ (Figure 3) to the head of a breakwater at $t/T = 1/2$ (Figure 5). It is noted that the magnitude of maximum pore pressure does not vary as the time changes.

Figures 7-10 illustrates the contour distributions of the vertical effective normal stresses (σ'_z/p_o) for various time intervals at $z = -1$ m. The figure indicates that the vertical effective normal stress (σ'_z/p_o) has a phase difference of $\pi/2$ from the pore pressure, as shown in Figures 3-10. That is, a negative vertical effective normal

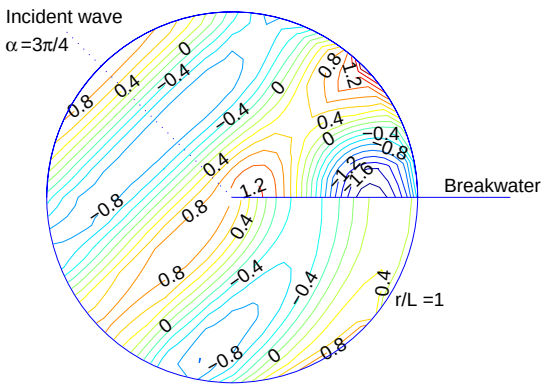

Figure 3: Contours of the wave-induced pore pressure (p/p_o) at z =-1 m for various time itervals. ($\alpha = 3\pi/4$, $K = 10^{-2}$ m/sec, G =10^7 N/m^2 and t/T=0).

stress occurs at the head of a breakwater when $t/T = 0$, while it is positive when $t/T = 1/2$.

Referring to Figure 1, Figures 3-10 demonstrate the significant effects of diffracted waves on the pore pressure distribution near the head of a breakwater, compared with that in front of a breakwater (i.e., Zone A in Figure 1).

2.4.2 Wave obliquity

The wave obliquity is another factor which only exists in three-dimensional cases. The vertical distributions of the wave-induced pore pressure (p/p_o) and vertical effective normal stress (σ'_z) versus relative soil depth (z/h) for various locations in raidal direction (θ-direction) with different incident wave angles ($\alpha = \pi/4$, $\pi/2$, $3\pi/4$ and π) at $r/L = 0.1$ are presented in Figures 11-18. In the figures, several locations in the θ-direction are chosen, i.e., $\theta = 0$, $\pi/4$, $\pi/2$, $3\pi/4$, π, $5\pi/4$, $3\pi/2$, $7\pi/4$ and 2π. In the case of $\alpha = \pi$ (Figures 14 and 18) are identical. As shown in the figure, the magnitude of the pore pressure and vertical effective normal stresses decrease as the θ increases, as the wave-induced pore pressure gradually decreases from front of a breakwater to rear of a breakwater. This trend is obvious at $\alpha = \pi/4$, and becomes less obvious as α increases.

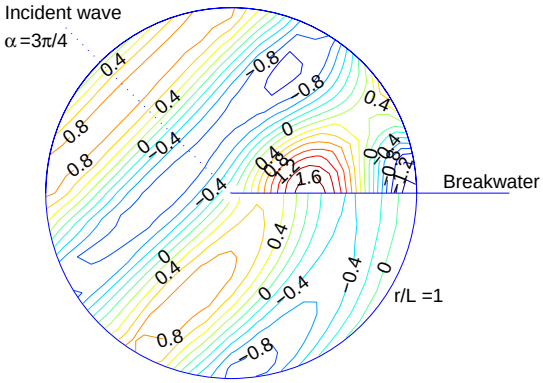

Figure 4: Contours of the wave-induced pore pressure (p/p_o) at z =-1 m for various time itervals. ($\alpha = 3\pi/4$, $K = 10^{-2}$ m/sec, G =10^7 N/m^2 and t/T=1/4).

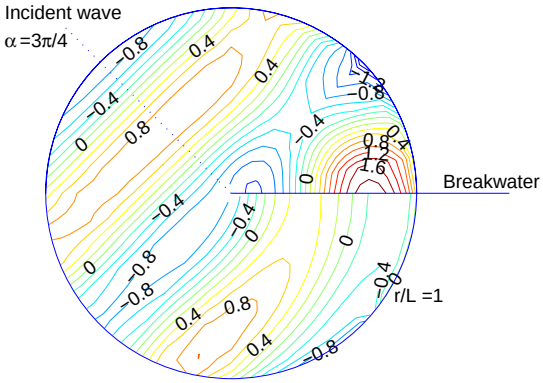

Figure 5: Contours of the wave-induced pore pressure (p/p_o) at z =-1 m for various time itervals. ($\alpha = 3\pi/4$, $K = 10^{-2}$ m/sec, G =10^7 N/m^2 and t/T=1/2).

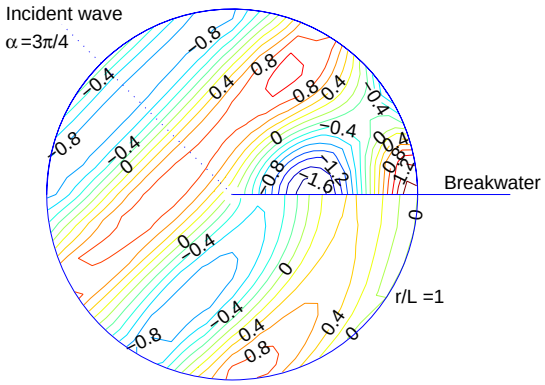

Figure 6: Contours of the wave-induced pore pressure (p/p_o) at z =-1 m for various time itervals. ($\alpha = 3\pi/4$, $K = 10^{-2}$ m/sec, G =10^7 N/m^2 and t/T==3/4).

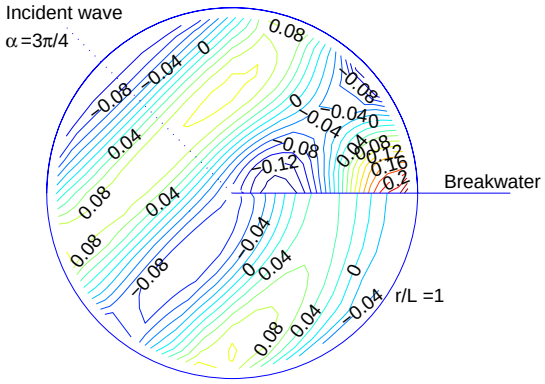

Figure 7: Contours of the wave-induced vertical effective normal stresses (σ'_z/p_o) at z =-1 m for various time itervals. ($\alpha = 3\pi/4$, $K = 10^{-2}$ m/sec, G =10^7 N/m^2 and t/T=0).

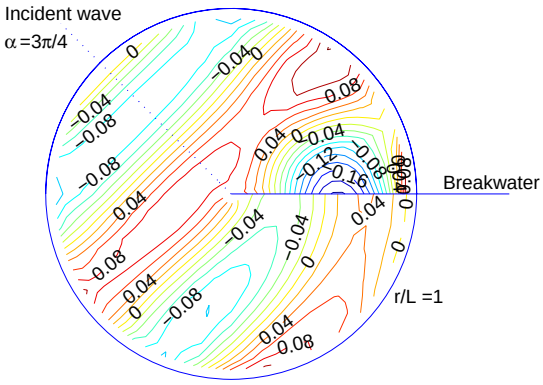

Figure 8: Contours of the wave-induced vertical effective normal stresses (σ'_z/p_o) at z =-1 m for various time itervals. ($\alpha = 3\pi/4$, $K = 10^{-2}$ m/sec, G =10^7 N/m^2 and t/T=1/4).

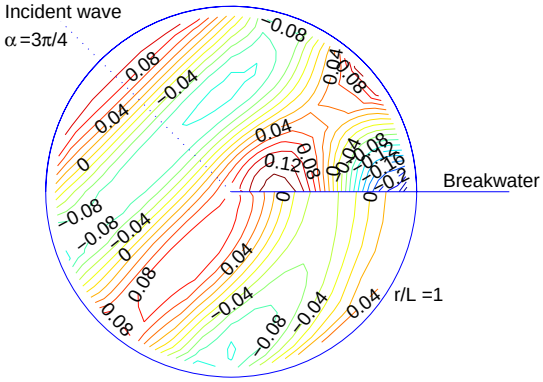

Figure 9: Contours of the wave-induced vertical effective normal stresses (σ'_z/p_o) at z =-1 m for various time itervals. ($\alpha = 3\pi/4$, $K = 10^{-2}$ m/sec, G =10^7 N/m^2 and t/T=1/2).